The Electrochemical Corrosion Behaviour of Q235 Steel in Soil Containing Sodium Chloride

Yujie Lan, Honglin Chang, Gang Qi, Pengju Han, Bin He[*]

College of Civil Engineering, Taiyuan University of Technology, Taiyuan, 030024, China
[*]E-mail: hebin@tyut.edu.cn

In this paper, the silt soil in Shanxi, China was selected and sodium chloride solution was added to the soil as the simulated saline soil. The corrosion characteristics of four contaminated soils with various sodium chloride contents were analysed by electrochemical impedance spectroscopy (EIS), and the electrochemical corrosion behaviour of Q235 steel at three ages in these four different simulated saline soil environments was studied by using EIS and polarization curves. The corrosion mechanism was analysed by scanning electron microscopy (SEM). The test results showed that the soil with a sodium chloride content of 2.3% had the strongest electrical conductivity. The increase in the sodium chloride content in the soil promoted not only the conductivity and corrosiveness of the soil but also the corrosion rate of Q235 steel. By fitting the electrochemical impedance spectra of steel, two equivalent circuits of R(CR(QR))(CR) and LR(QR)(QR) were obtained, and the total impedance formulas were deduced. By analysing the parameters of the equivalent circuit, the corrosion process of Q235 steel was determined. The corrosion area on the surface of the Q235 steel specimen continued to expand, and the degree of corrosion deepened with increasing sodium chloride concentration in the soil.

1. INTRODUCTION

China's saline soil has a large distribution span. As shown in Figure 1, saline soil is distributed in the central and western regions as well as the coastal areas of China. Saline soil will bring a series of adverse effects, such as inhibiting the growth of plants, and causing corrosion of building components in the soil. [1-3]. China consumes many resources every year to solve various problems caused by corrosion; according to statistics, the total cost of corrosion in China in 2014 alone exceeded 2.1 trillion RMB, accounting for approximately 3.34% of that year's GDP. Globally, the total cost of corrosion is more than 4 trillion US dollars per year, which is 40 times the losses caused by Hurricane Katrina. [4].

Among the various salt types, chloride salt is the main salt that causes metal corrosion in saline soil. Some studies have found that sand that contains sodium chloride is the most corrosive compared with sand containing Na_2SO_4 and $NaHCO_3$ [5]. Among all types of steel, Q235 steel has moderate carbon and has good performance. It is widely used in construction and engineering structures [6-7]. The "Technical Standard for Prestressed Concrete Pipe Piles" (JBJ/T 406-2017) of China stipulates that the end plate material of prestressed high strength concrete (PHC)) should be Q235B steel. PHC pipe piles are used in construction fields such as real estate, port terminals, and airport construction. The sales of PHC pipe piles in China in 2018 reached approximately 295 million metres. In recent years, with the promotion of China's Western Development Policy and the One Belt One Road Strategy, a large number of infrastructure projects have moved to the central and western regions. However, soil salinization has seriously affected the implementation and service life of construction projects. As a result, soil salinization severely restricts the development of the region. Therefore, it is important to study the corrosivity of polluted soils with different sodium chloride contents and investigate the corrosion mechanism of Q235 steel in simulated saline soil to extend the service life of PHC pipe pile endplates and support the conservation and utilization of resources in China and throughout the world.
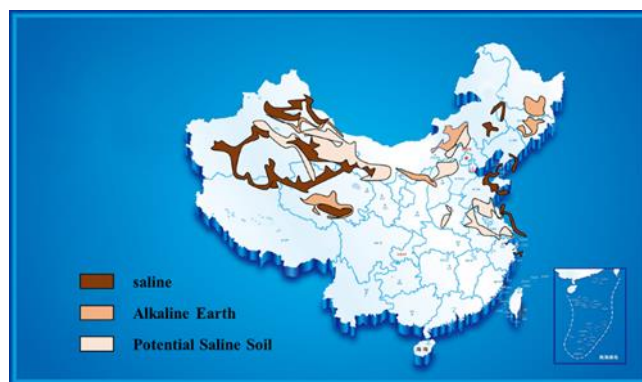
Figure 1. Distribution map of saline soil in China.

Recently, many scholars around the world have proposed research on the corrosion behaviour of soil; based on this fact, some scholars have proposed effective methods to evaluate soil corrosivity [8-9] and studied the electrochemical corrosion behaviour of steel in polluted soil environments. Some important conclusions were derived from these studies. I.S.Cole [10] performed a comprehensive review on the changes in soil corrosion and the metal corrosion rate. Zuo [11] simulated the impact of acid rain on the corrosion behaviour of Q235 steel in acidic soils. Researchers have found that the corrosion rate increases as the pH value of simulated acid rain decreases, but as the test time increases, the impedance increases and the corrosion rate decreases. Zhu [12] studied the corrosion behaviour of Q235 steel in three typical soil environments. The experimental results show that higher concentrations of OH^-, Ca^{2+}, Mg^{2+} and other cations in alkaline saline-alkaline soil are beneficial to the formation of metal oxides. Xu [13] studied the corrosion behaviour of Q235 steel in a simulated solution of weakly alkaline soil in Wuhan. The researchers found that the increases in $SO4^{2-}$ and Cl^- concentrations above the critical

concentration would weaken the passivation performance of Q235 steel. Some scholars have studied the buried corrosion of pipeline steel. The results of the study have shown that soil pH, water content, temperature, time, ions, and microorganisms all affect the corrosion behaviour of pipeline steel [14-26]. Muhammad Wasim [27] proposed a more comprehensive review on the factors that cause the corrosion of buried pipes. D. M. Wei [28] studied corrosion on welded joints of PHC pipe piles but did not consider the impact of soil. B. L. Lin [29] investigated the corrosion behaviour of the metal end of PHC pipe piles in four types of soil simulation fluids. The results showed that the corrosion rates of the Q235 steel endplate and Z9 steel main reinforcement in saline soil were greater than those in non-saline soil.

To the best of our knowledge, few studies have been proposed on the corrosion behaviour and mechanism of Q235 steel in loess-like silt polluted by different sodium chloride concentrations. Thus, in this paper, we use indoor simulated saline soil experiments to bury Q235 steel samples in four contaminated soils with different sodium chloride contents. By using EIS, polarization curves and SEM images, we performed a comprehensive analysis of simulated saline soil with different sodium chloride contents and the electrochemical corrosion behaviour of Q235 steel in a saline soil environment, and its corrosion mechanism was revealed.

2. EXPERIMENTAL

2.1 Sample and Contaminated Soil Preparation

Table 1. Q235 steel chemical composition

Chemical Composition	C	Si	Mn	P	S	Al
Content /%	0.20	0.10	0.14	0.021	0.003	0.01

The test piece was selected from Q235 steel and cut into 1.5 cm×1.5 cm×2 cm steel sheets. The chemical composition of Q235 steel is shown in Table 1. First, we ground the steel sheets step by step with 800-1500 grit sandpaper. Second, we cleaned them in absolute ethanol and removed them for blow-drying. Third, we wrapped copper wires around the thickness of the steel sheets and leave 1 cm×1 cm on one side of the steel sheets. The rest of the working surface was sealed with epoxy resin to ensure that the copper wire was not exposed but there were four steel samples without sealing treatment, which were used to observe the macro and micromorphology after 60 days of corrosion.
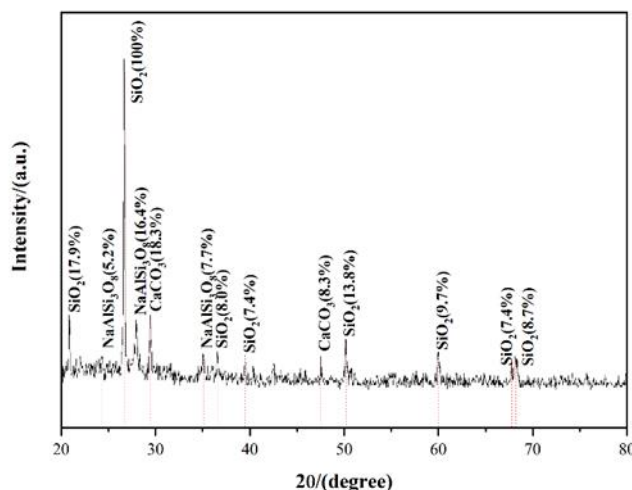
Figure 2. XRD spectrum of silt.

The silt soil sample was taken from a construction site in Shanxi. The X-ray diffraction (XRD) spectrum of the silt soil sample is shown in Figure 2. The major components of the silt soil are SiO_2, $NaAlSi_3O_8$, and $CaCO_3$. First, we used the drying method to measure the moisture content ω of the soil and obtained $\omega=1.08\%$. Second, we dried all of the required soil samples in an oven and took a part of the dried soil to measure the liquid limit ω_L and plastic limit ω_P. We got the results $\omega_L=28.7\%$ and $\omega_P=19.0\%$ by using a liquid-plastic combine tester. The plasticity index I_P of the sample was calculated to be 9.7. Third, we dried the remaining soil and passed it through a 1 mm sieve. After this procedure, we prepared a sodium chloride solution that was mixed into the dry silt soil. According to the Chinese "Geotechnical Engineering Survey Specification" (GB-50021-2001), rock-soil should be judged as saline soil when the soluble salt content is greater than 0.3% and has engineering characteristics such as collapsibility, salt expansion and corrosion. Additionally, based on the Chinese "Soil Test Method Standard" (GB/T 50123—2019), the calculation formula for the soil salt content is Eq. (1):

$$m = \frac{m_1}{m_0} \times 100\%$$

Eq. (1)

where m_1 is the quality of salt (chlorine, sulfate, carbonate) in the soil, and m_0 is the air-dried soil weight. The amount of water added for the water content of the soil sample preparation is based on the standard Eq. (2):

$$m_w = \frac{m_0}{1+0.01m_0} \times 0.01\left(\omega'-\omega_0\right)$$

Eq. (2)

where m_0 is the air-dried soil weight, m_w is the amount of water needed to be added to the soil sample, ω' is the required moisture content, and ω_0 is the air-dried moisture content.

We use Eqs. (1) and (2) to calculate the sodium chloride weight that will be added to the solution. The purpose of adding sodium chloride solution to the soil sample is to mimic the saline soil

environment. In summary, the ratio of the soil sample is shown in Table 2, and the soil sample was mixed well manually.

Table 2. Proportions of soil samples with different sodium chloride contents

Moisture Content /%	Salt Content/%	Quantity of Oven-Dried Soil /g	Quantity of High Purity Sodium Chloride Powder/g	Quantity of Water Added to Oven-Dried Soil /g
24	0	2000	0	453.5
	0.3	2000	6.0	453.5
	1.3	2000	26.0	453.5
	2.3	2000	46.0	453.5

2.2 Experimental Method

There were two sets of parallel samples for each type electrochemical corrosion test piece, plus four test pieces for macro and micro testing. Therefore, a total of 12 test pieces were prepared. First, we put copper sheets of the same width as the soil tank on both sides of the soil tank as inert electrodes to measure the impedance of the soil contaminated by different sodium chloride contents. Second, we loaded the prepared soil sample into a 7.07 cm×7.07 cm×7.07 cm soil sample tank and used an artificial compaction method to ensure compactness. When we filled the tank with soil to a height of 3 cm, we placed the 1 cm×1 cm exposed side of the steel sheet sample for electrochemistry parallel to the copper sheet. After that, we continued to add soil to compact the height to 6.5 cm of the soil sample tank.

We used a CS350 electrochemical workstation to evaluate the electrochemical performance of the corrosion process. Relying on the CS350 workstation to measure the EIS of sodium chloride contaminated soil, the EIS and polarization curve of Q235 steel were determined. The measurement frequency range of EIS was 10^{-2}~10^{5} Hz, the sweep frequency mode adopteds the linear logarithmic sweep method, and the applied sine wave amplitude was 10 mV. The scan rate used when testing the polarization curve is 2 mV/s. When measuring the EIS of sodium chloride contaminated soil, first, the soil was allowed to stand for one day after the burying process was completed. Then, the workstation was connected to the electrode. The working schematic diagram is shown in Figure 3(b), There are 7.07 cm copper sheets with the same width as the two sides of the soil trough on both sides of the soil trough, one of which was used as a working electrode (WE) when measuring the electrochemical impedance of the soil, and the other end was used as the counter electrode (CE) and the reference electrode (RE). Finally, after the potential of the working electrode to be connected was stable for 30 minutes, the EIS of soil contaminated with sodium chloride contents of 0, 0.3, 1.3, and 2.3% was measured at a moisture content of 24%. Then, we measured the EIS and polarization curves of Q235 steel sheets when the Q235 steel sheets were buried for 14, 28, and 60 days, as shown in Figure 3 (a) and (b). When measuring the EIS and polarization curve of the Q235 steel sheet, we used copper wires wrapped with the steel sheet as the WE and two 3.5 cm wide copper sheets as the CE and RE. Similarly, the EIS of Q235 steel was measured after the potential of the working electrode to be connected was stable for 30 minutes. When

the open circuit potential of the metal electrode reached a stable state, the polarization curve test was started, sweeping from the cathode part of the polarization curve to the open circuit potential, and finally to the anode part of the polarization curve. After each test, we covered the surface of the soil tank with a multilayer waterproof breathable membrane to prevent moisture loss. We then analysed and fit the measured EIS by using ZView and ZSimDemo, and we also analysed the polarization curve by using CView. When the steel sheets had been buried for 60 days, the steel sheets were removed from the soil samples. The soil attached to the samples was removed with anhydrous ethanol, the samples were blown dry with a rubber suction bulb. Then, SEM was used to observe the micromorphology of the steel sheet after corrosion. SEM was performed using a TM3000 desktop scanning electron microscope produced by the HITACHI Company (Japan). The magnification range of the instrument is 30~10000 times. The degree of corrosion of Q235 steel in soil contaminated with different sodium chloride contents was determined and the corrosion mechanism was analysed.
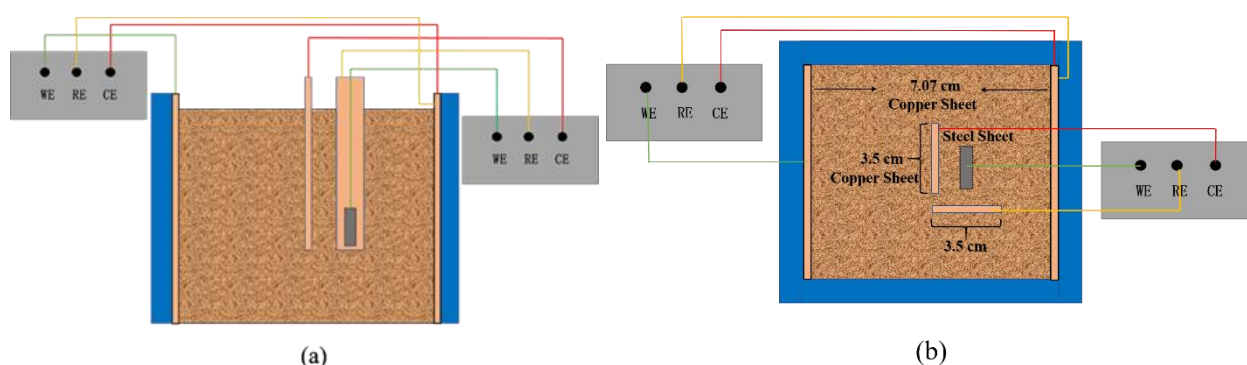
Figure 3. Test device diagram. (a) Front view of the test device and, (b) top view of the test device

3. RESULTS AND DISCUSSION

3.1 Electrochemical impedance spectroscopy of soil containing sodium chloride

Electrochemical tests were performed on soils with a moisture content of 24% and sodium chloride contents of 0%, 0.3%, 1.3%, and 2.3%. The impedance spectrum test results are shown in Figure 4. The Nyquist diagrams of the four soils with various sodium chloride contents are all composed of incomplete capacitive reactance arcs in the high-frequency region, and there is no diffusion impedance. The starting point of the Nyquist pattern of the uncontaminated soil is the far right, and with the increase of sodium chloride content, the starting point of the capacitive resistance arc moves to the left, while the diameter gradually decreases, indicating that with the increase of the sodium chloride content, the resistance of the solution electrolyte in the soil pores decreases, the charge transfer resistance will also decrease as the concentration increases. Therefore, with a content of 2.3% sodium chloride silt soil has the strongest conductivity and the strongest corrosiveness. Obviously, the impedance modulus of the uncontaminated soil in the Bode diagram (F-|Z|) is much larger than that of the contaminated soil, and

as the sodium chloride content increases successively, the impedance modulus decreases, again indicating that as the sodium chloride content increases, the soil conductivity and corrosion increase. In the Bode diagram (log F-θ), there is only one peak in the graphs of unpolluted soil [30] and soil with sodium chloride content of 0.3%, and there is only one time constant in the electrochemical process; however, in the graphs for soils with 1.3% and 2.3% sodium chloride contents there are two peaks, which indicates that there are two time constants.
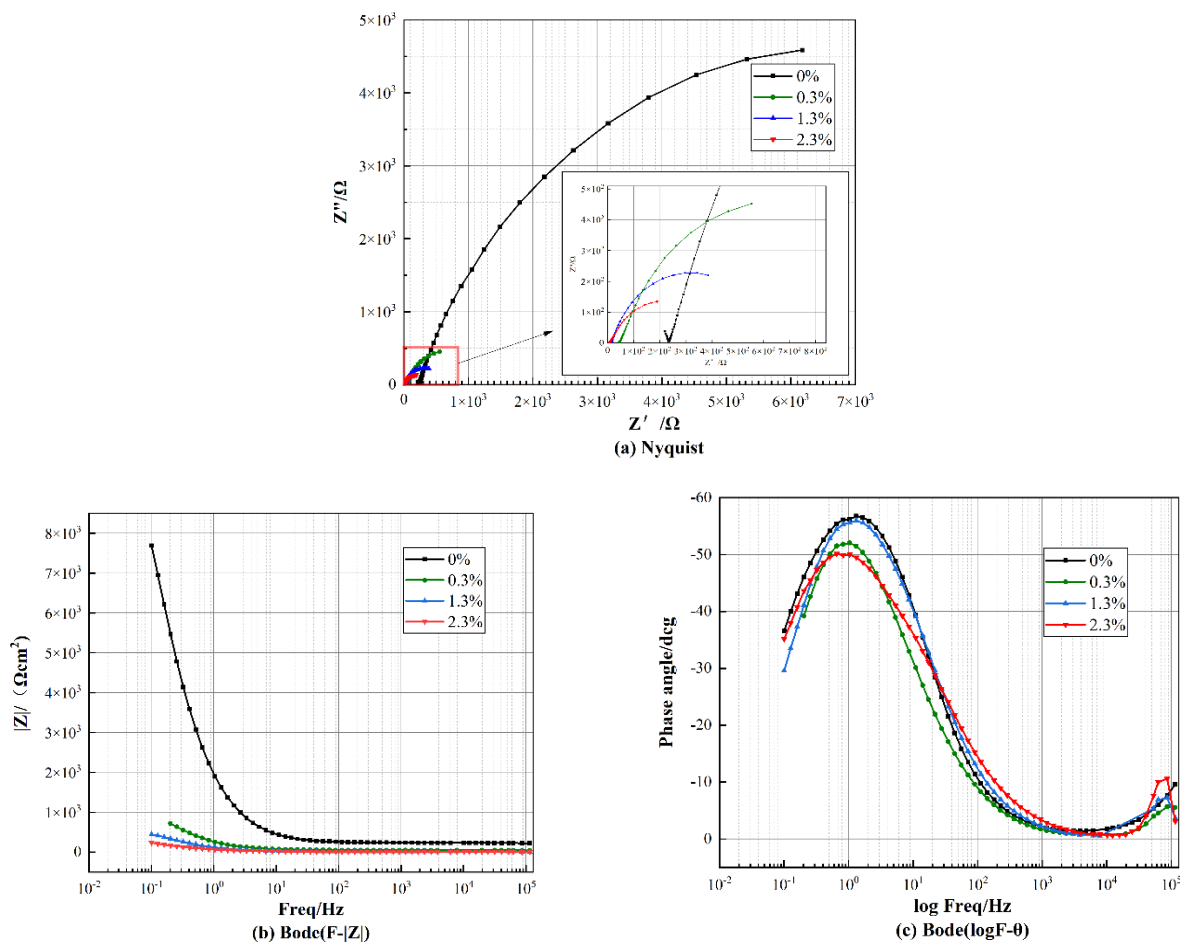
Figure 4. (a) Nyquist diagram of soil with 0,0.3,1.3, and 2.3% sodium chloride contents, (b) Bode(F-|Z|) diagrams of soil with 0,0.3,1.3, and 2.3% sodium chloride contents, and (c) Bode (logF-θ) diagrams of soil with 0,0.3,1.3, and 2.3% sodium chloride contents

Silt is composed of three states: solid, liquid and gas, and thus, there are three conductive paths inside the soil. They are: (1) the conduction between soil particles; (2) the conduction of pore fluid; and (3) the conduction between soil particles and the contact surface of the pore solution [31]. The electrochemical impedance spectroscopy graph was fitted by ZSimDemo software, and the effect of the R(Q(R(CR))) type equivalent circuit was obtained. The equivalent circuit diagram is shown in Figure 5. In the process of current transmission, there is the resistance R_L of the electrolyte in the pore solution of the soil particles. Due to the addition of copper electrodes at both ends of the soil, the discontinuous contact between the silt particles and the surface of the copper electrode causes a dispersion effect; in

the fitted equivalent circuit, the constant phase angle element Q is used to replace the electric double layer capacitor. R_S and C_S are the resistance of the silt layer and the capacitance of the soil particles respectively, which are connected in parallel [32]. R_{ct} is the charge transfer resistance, and its value reflects the difficulty of charge transfer between the electrode and the electrolyte interface.
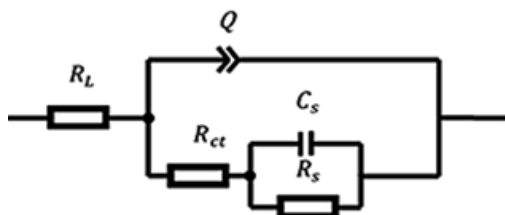
Figure 5. Equivalent circuit diagram of sodium chloride simulated saline soil

Table 3. Soil equivalent circuit parameters

Salt Content/%	$R_L/\Omega \cdot cm^2$	$Y_0/S \cdot s^{-n} \cdot cm^{-2}$	n	$R_s/\Omega \cdot cm^2$	C_s	$R_{ct}/\Omega \cdot cm^2$
0	231.70	1.147×10^{-4}	0.7430	81.26	1.111×10^{-5}	13630.00
0.3	46.26	7.943×10^{-4}	0.7743	241.10	1.361×10^{-4}	1058.00
1.3	14.05	1.719×10^{-3}	0.7885	164.00	2.237×10^{-4}	469.00
2.3	8.65	3.854×10^{-3}	0.6929	130.40	5.643×10^{-4}	320.40

The equivalent circuit parameters are shown in Table 3. The R_L value of uncontaminated silt soil is the largest at 231.70$\Omega \cdot cm^2$, which is approximately 27 times the resistance value of the soil with a 2.3% sodium chloride content. It is related to the ion concentration of the pore solution and the porosity of the soil. Since the sodium chloride content of the soil in this experiment is different, other conditions are the same, and R_L is inversely proportional to the ion concentration in the solution, which results in the R_L value decreasing as the sodium chloride content increases. The silt soil used in the test passes through a 1 mm sieve, and the particle size of the soil particles is small. After artificial compaction, the soil is dense, and the electric charge is more impeded in the transfer process of the silt than in the sand, therefore, the R_{ct} value is generally larger. The resistance value of the uncontaminated soil even reached 13630$\Omega \cdot cm^2$, which is an order of magnitude larger than the resistance value of the 0.3% content, and 42 times the resistance of the 2.3% content, and it continues to decrease with increasing sodium chloride content. The clay particles in the silt are in full contact with the aqueous solution. An electric field will be formed around the negatively charged clay particles to adsorb surrounding cations (such as Na+), thus forming a diffuse electric double layer on the surface of the particles. Therefore, there is an electric double layer capacitance C_s during the electrification process, and with the increase in sodium chloride content, the number of cations increases, and the force between the surface of the soil particles and the solution also increases. The resistance of the silt layer should decrease with increasing sodium chloride content, but the test results show that the resistance value is the smallest in the uncontaminated soil,

which is due to the lack of part of the resistance value of the ions in the sodium chloride solution. The constant phase angle element Q reflects a nonideal capacitance, which is equivalent to the double-layer capacitance at the interface between the electrode and the soil. This is because the surface of the copper electrode in the soil with a large sodium chloride content will react with Cl⁻ to form $CuCl_2$, and the value of n is 0.6 ~0.8, indicating that it is not close to the ideal capacitance. In summary, the fitting results mentioned above are consistent with the electrochemical impedance spectroscopy, which also shows that the increase of the sodium chloride content in the simulated saline soil promotes the conductivity of the soil and increases the corrosion of the soil.

3.2 Polarization curve of Q235 steel

(a)

(b)
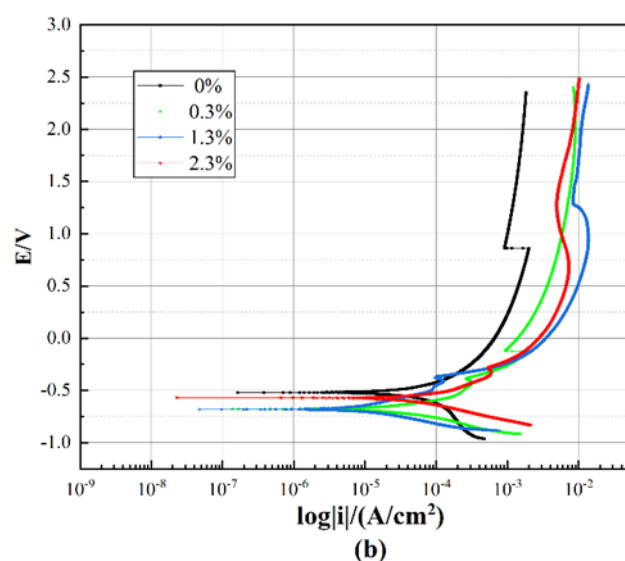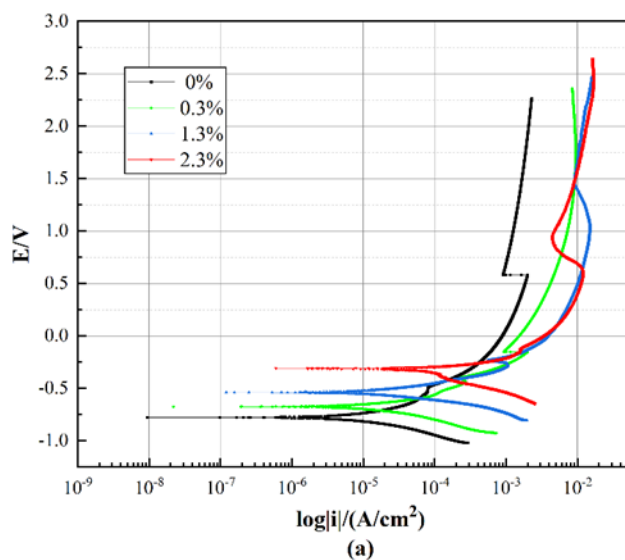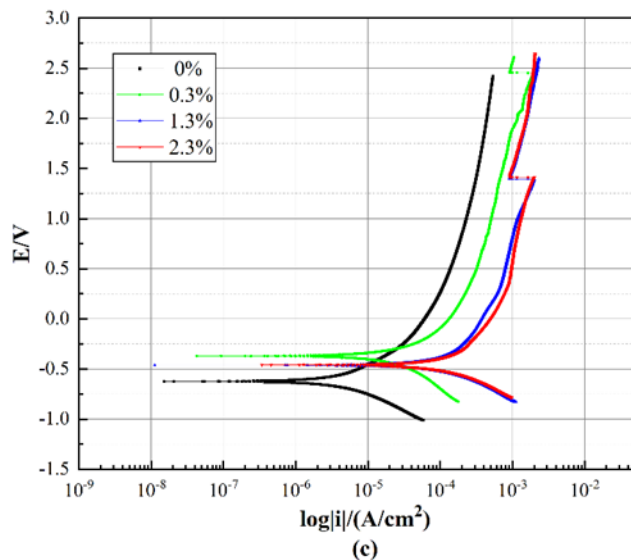
Figure 6. Polarization curves of Q235 steel buried in silt soil with sodium chloride contents of 0, 0.3, 1.3, and 2.3% for 14 days (a), 28 days (b), and 60 days (c)

Figure 6 (a), (b) and (c) show the polarization curves of the Q235 steel samples buried in soil with a 24% moisture content and different sodium chloride contents for 14, 28, and 60 days, respectively. The upper part of the bifurcate curve represents the anodic polarization process, where an oxidation reaction occurs at the anode. The chemical reaction formula is shown in Eq. (3). The lower part of the bifurcate curve represents the cathodic polarization process, where a reduction reaction occurs at the cathode. The chemical reaction formula is shown in Eq. (4).

$$2Fe \rightarrow 2Fe^{2+} + 4e$$

Eq. (3)

$$O_2 + 2H_2O + 4e \rightarrow 4OH^-$$

Eq. (4)

We find that there is little change in the cathode part. However, the electrode dissolution step, that is, the passivation zone, appears in the anode. As shown in all of the curves of Figure 6 (a), at 14 days, the self-corrosion potential E_{corr} increases with increasing sodium chloride content. The E_{corr} of the steel sheet in the uncontaminated soil is at the most negative position, which indicates that its corrosion thermodynamic trend is relatively large, and the steel sheet is easily corroded at this time. The polarization curve of the steel sheet in the soil with 2.3% sodium chloride is at the top; at this time, the steel sample has better corrosion resistance, which is related to the obvious passivation at 2.3% content. The passivation process is an important factor affecting the corrosion rate, and the corrosion rate suddenly decreases after passivation occurs. This is because the steel sheet corrosion products Fe_3O_4 and Fe_2O_3 formed on the surface hinder the progress of corrosion, and the anode electrode process is subject to greater resistance. This type of electrochemical corrosion phenomenon occurs in both pipeline steel and mild steel. [33-35], which hinders the dissolution of steel, and no longer obeys Tafel's kinetic law. In general, the occurrence of passivation process is roughly divided into four parts. (1) Activation zone. The anode obstruction is small and still obeys Tafel's law, and the reaction process is shown in Eq. (5).

(2) Transition zone. At this time, the current density is the largest, sign passivation begins, anode obstruction increases, and it starts to deviate from Tafel's law. The surface gradually generates unstable oxides or corrosion products, and the reaction process is shown in Eq. (6). (3) Stable passivation area. The current density is basically unchanged at this time, but corrosion still takes place, forming a passivation film with better corrosion resistance, and the reaction process is shown in Eq. (7). (4) Passivation zone. The corrosion-resistant oxides produced before are further oxidized and become non-corrosive compounds, and the corrosion is further intensified.

$$Fe \rightarrow Fe^{2+} + 2e$$

<div align="right">Eq. (5)</div>

$$3Fe + 4H_2O \rightarrow Fe_3O_4 + 8H^+ + 8e$$

<div align="right">Eq. (6)</div>

$$2Fe + 2H_2O \rightarrow \gamma - Fe_2O_3 + 6H^+ + 6e$$

<div align="right">Eq. (7)</div>

As the sodium chloride content increases, the starting point of the curve also shifts to the right, and the corrosion current density I_{corr} continues to increase. The lower part of the bifurcate curve represents the cathodic polarization process, where reduction reaction occurs at the cathode. The chemical reaction formula is shown in Eq. (4).

The steel sheet in the soil with a 2.3% sodium chloride content shows the largest corrosion kinetic trend and the fastest corrosion rate (see Figure 6 (a)). As shown in Figure 6 (b), the I_{corr} and E_{corr} of all the polarization curves of Q235 steel in the four soil samples with various sodium chloride contents are similar at 28 days. The polarization curve of the steel sample corrosion for 60 days is shown in Figure 6(c); compared with the polarization curve at 28 days, the polarization curve of Q235 steel in the uncontaminated soil is obviously shifted downward. At this time, the steel sheet easily corrodes, but the polarization curve of the steel in the contaminated soil containing sodium chloride is shifted upward. The corrosion thermodynamic trend of steel in the soil containing sodium chloride is reduced, the corrosion tendency is reduced, and the steel surface is gradually resistant to corrosion. The situation is similar to 14 days, which is related to the obvious passivation of the steel surface. It is worth noting that, compared with the other three curves, the polarization curve of steel in 2.3% sodium chloride silt is obviously on the right. At this time, the corrosion kinetics trend of the steel plate in 2.3% sodium chloride soil is the largest, and the corrosion rate is the fastest. This trend is similar to that of 14 days, indicating that under the same number of corrosion days, when the sodium chloride content in the soil reaches a certain level, sodium chloride can promote the soil electrical conductivity and accelerate the corrosion rate of Q235 steel, which is confirmed by the abovementioned soil impedance conclusion.

Table 4. Polarization curve fitting parameters of Q235 steel

Time	Salt Content/%	B_a/(mV/dec)	B_c/(mV/dec)	I_{corr}/ (A/cm^2)	E_{corr}/V	Corrosion Rate/(mm/a)	Corrosion Grade
14 days	0	178	145	8.279×10^{-6}	-0.778	0.097	Medium
	0.3	141	149	1.468×10^{-5}	-0.674	0.172	Serious
	1.3	105	90	1.411×10^{-5}	-0.540	0.165	Serious
	2.3	82	145	3.211×10^{-5}	-0.311	0.375	Extremely Serious
28 days	0	526	635	1.229×10^{-4}	-0.520	1.436	Extremely Serious
	0.3	144	140	2.462×10^{-5}	-0.678	0.288	Extremely Serious
	1.3	233	145	1.482×10^{-5}	-0.682	0.138	Serious
	2.3	222	256	8.461×10^{-5}	-0.570	0.989	Extremely Serious
60 days	0	832	479	9.418×10^{-6}	-0.623	0.111	Medium
	0.3	395	563	3.104×10^{-5}	-0.371	0.365	Extremely Serious
	1.3	925	392	1.705×10^{-4}	-0.463	2.006	Extremely Serious
	2.3	715	395	1.804×10^{-4}	-0.458	2.122	Extremely Serious

Table 5. Corrosion grade evaluation table (Ref 36)

I_{corr}/(μA/cm^2)	Degree of Corrosion	Corrosion Grade
<3	Slight	First Level
3~10	Medium	Second Level
10~20	Serious	Third Level
>20	Extremely Serious	Fourth Level

The parameters obtained by fitting the polarization curve through CView software are shown in Table 4, in which the corrosion level is determined according to the corrosion level evaluation in Table 5 [36]. According to the evaluation, Q235 steel suffered extremely severe corrosion when it was buried in all contaminated soil containing sodium chloride for 60 days. It can be seen from the fitted values that the I_{corr} and corrosion rate of the Q235 steel sample in uncontaminated soil first increase and then decrease with the increase of days, while in the soil containing sodium chloride, the I_{corr} and corrosion rate increase with the increase in the number of days. It is worth pointing out that the I_{corr} of Q235 steel in uncontaminated soil will decrease with the increase of the number of corrosion days rather than increase with the increase in the number of corrosion days. However, the I_{corr} of Q235 steel in the soil

containing sodium chloride will show an increasing trend with the increase in the number of corrosion days.

3.3 Electrochemical impedance spectroscopy of Q235 steel
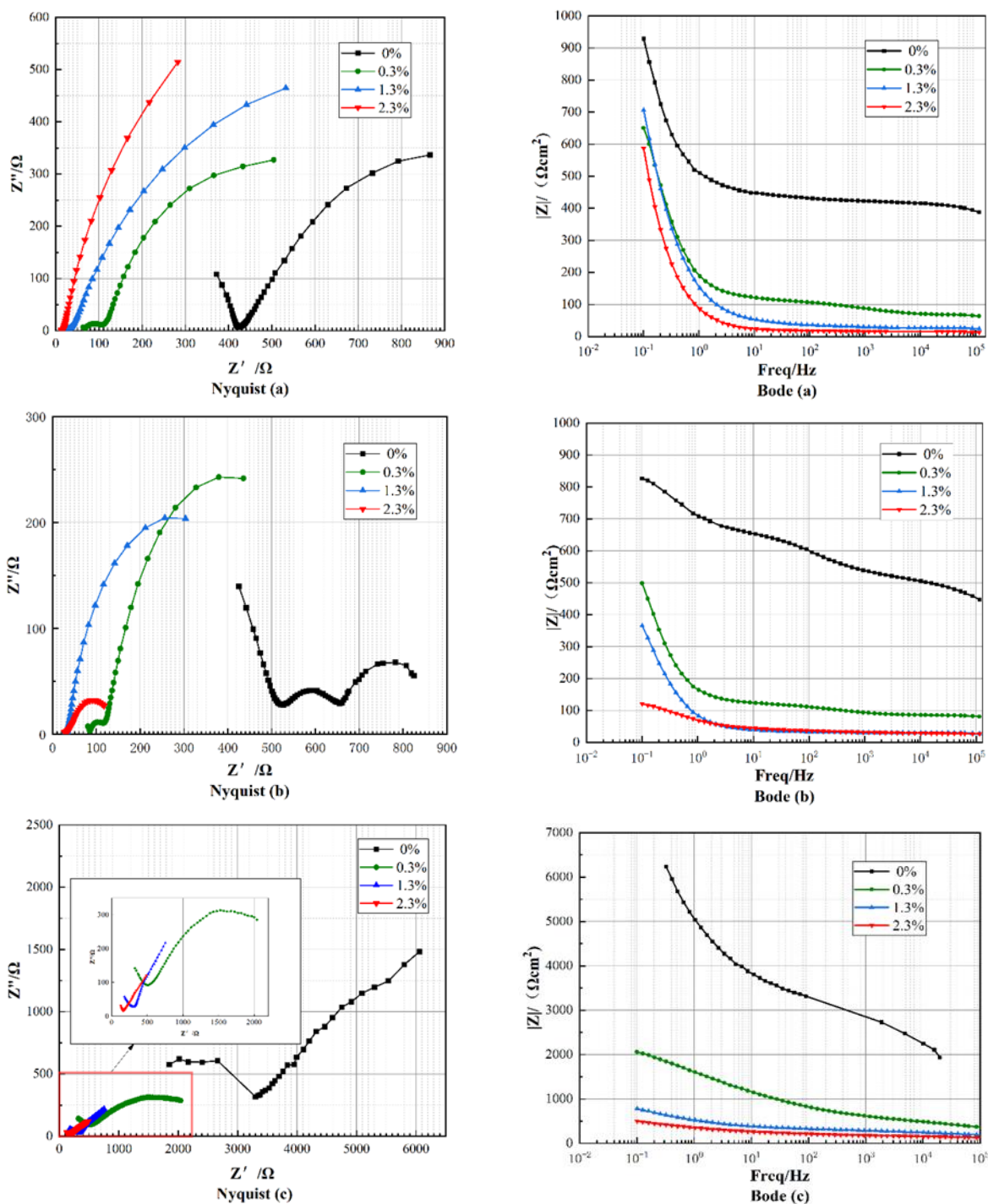
Figure 7. Nyquist diagrams and Bode diagrams of Q235 steel buried in silt soil with sodium chloride contents of 0, 0.3, 1.3, and 2.3% for 14 days(a), 28 days(b) and 60 days(c)

Figures 7 (a), (b) and (c) show the Nyquist diagrams and Bode diagrams of Q235 steel in silt soil with different sodium chloride contents at 14, 28, and 60 days respectively. In Figure 7, the Nyquist diagram of Q235 steel in uncontaminated soil shows double capacitive resistance arcs and relatively complete capacitive resistance arcs in the low-frequency region at 28 and 60 days. This is because the process of preventing steel sheet corrosion occurs during the corrosion process of Q235 steel. The Nyquist diagram of Q235 steel buried in 2.3% sodium chloride -contaminated silt for 60 days shows that in the low-frequency region, a straight line with an inclination angle of approximately 45° appears, which is caused by the diffusion process. All graphs of the Bode diagram have similar changing trends. The low-frequency area is composed of oblique lines with an inclination of approximately 135°, the high-frequency area is composed of straight lines roughly parallel to the horizontal axis, and with the increase of the sodium chloride content in the soil, the |Z| value gradually decreases.The corrosion resistance of steel decreased as the content of sodium chloride increasing. At 60 days, the overall |Z| value increased by approximately an order of magnitude.
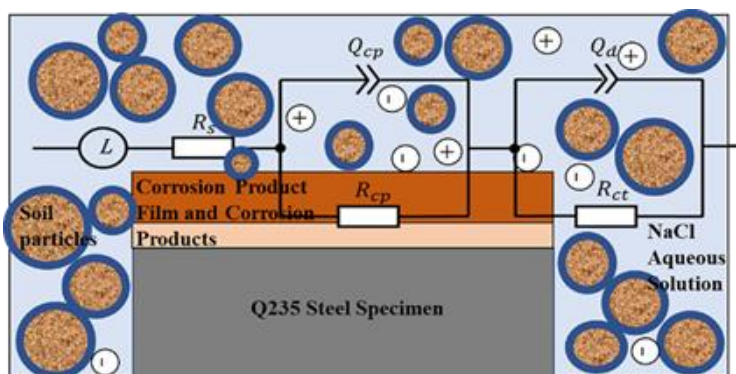
Figure 8. Equivalent circuit diagram of Q235 steel in uncontaminated soil

Table 6. Equivalent circuit parameters of Q235 steel in uncontaminated soil

Time	Salt Content /%	$R_s/\Omega \cdot cm^2$	C_{cp}/F	$R_{cp1}/\Omega \cdot cm^2$	Q_{dl}		$R_{cp2}/\Omega \cdot cm^2$	C_s/F	$R_{ct}/\Omega \cdot cm^2$
					$Y_0/S \cdot s^{-n} \cdot cm^{-2}$	n			
14 days	uncontaminated soil	117.5	2.05×10^{-9}	9808.0	5.205×10^{-3}	0.341	304.7	2.915×10^{-3}	445.9
28 days		102.7	1.585×10^{-9}	628.7	6.557×10^{-5}	0.365	868.6	4.028×10^{-3}	121.9
60 days		1233	8.625×10^{-8}	11630	1.405×10^{-4}	0.453	884.5	6.482×10^{-9}	1054

ZSimDemo software was used to fit the equivalent circuit diagrams and corrosion parameters of Q235 steel in uncontaminated soil for 14, 28 and 60 days, as shown in Figure 8 and Table 6. The fitting effect of the R(CR(QR)) (CR) equivalent circuit is good. Among them, the parameter R_s is the resistance of the uncontaminated silt layer, which increases significantly at 60 days. R_{ct} is the charge transfer resistance, which decreases significantly at 28 days, indicating that the charge transfer between the electrode and the electrolyte solution interface gradually becomes easy during the 28 days corrosion process of Q235 steel, which is consistent with the obtained polarization curve results. During this period, the corrosion rate of Q235 steel increases. R_{cp1} and R_{cp2} are the corrosion product film resistance

and corrosion product resistance, respectively. R_{cp1} decreases first and then increases with increasing corrosion time, but the R_{cp2} value increases with increasing corrosion time, indicating that the corrosion product film that hinders the corrosion of Q235 steel will be further oxidized into non-corrosive products, and then the non-corrosive products continue to react, which causes the corrosion products to continue to increase. C_{cp} is the corrosion product capacitance produced on the metal surface, and C_s is the electric double layer capacitance on the surface of the clay particles [37]. However, when the "dispersion effect" occurs during the corrosion process to form a nonideal capacitance, the Q_{dl} constant phase original element is used to replace the electric double-layer capacitance at the silt-steel interface. As the corrosion time increases, Q_{dl} decreases by one to two orders of magnitude, and n is between 0.3 and 0.5, which deviates from the ideal capacitance. Eq. (11) for calculating the total impedance of Q235 steel in uncontaminated soil is derived from Eqs. (8) (9) and (10).

$$Z = R_s + \cfrac{1}{\cfrac{1}{Z_{cp}} + \cfrac{1}{R_{cp1}} + \cfrac{1}{R_{cp2} + Z_Q}} + \frac{R_{ct}Z_s}{R_{ct} + Z_s}$$

Eq. (8)

$$Z_Q = [Y_Q(j\omega)^n]^{-1}$$

Eq. (9)

$$Z_{cp} = \frac{1}{\omega C_{cp}}, \quad Z_s = \frac{1}{\omega C_s}$$

Eq. (10)

$$Z = Rs + \frac{R_{cp1}Y_Q(\omega j)^n}{Y_Q(\omega j)^n [1 + R_{cp1}\omega C_{cp}] + R_{cp1}[1 + R_{cp2}Y_Q(\omega j)^n]} + \frac{R_{ct}}{\omega C_s R_{ct} + 1}$$

Eq. (11)

where Z_Q, Z_{cp}, and Z_s are the impedance of the constant phase element, the corrosion product capacitance, and the surface capacitance of the clay particles, respectively. Y_Q is a constant independent of frequency, $j = \sqrt{-1}$, and the angular frequency $\omega = 2\pi f$.
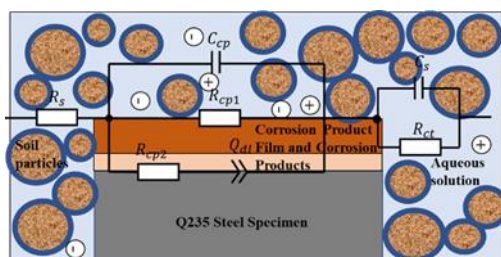
Figure 9. Equivalent circuit diagram of Q235 steel in sodium chloride contaminated soil

Table 7. Equivalent circuit parameters of Q235 steel in sodium chloride contaminated soil

Time	Salt Content /%	L/H·cm^2	R_s/Ω·cm^2	Q_{cp}		R_{cp}/Ω·cm^2	Q_{dl}		R_{ct}/Ω·cm^2
				Y_0/S·s^{-n}·cm^{-2}	n_1		Y_0/S·s^{-n}·cm^{-2}	n_2	
14 days	0.3	-	60.91	1.673×10^{-3}	0.883	781.80	3.448×10^{-4}	0.474	63.32
	1.3	-	24.40	1.686×10^{-3}	0.857	1130	1.014×10^{-2}	0.312	81.86
	2.3	-	10.15	2.394×10^{-3}	0.889	1971	2.395×10^{-3}	0.886	2008
28 days	0.3	-	81.04	2.528×10^{-3}	0.897	572.60	5.897×10^{-4}	0.504	49.37
	1.3	-	28.89	3.072×10^{-3}	0.921	444.80	2.921×10^{-2}	0.311	60.61
	2.3	-	25.14	8.754×10^{-3}	0.290	28.83	6.843×10^{-3}	0.759	89.17
60 days	0.3	-	5.86×10^{-5}	1.318×10^{-7}	0.694	398	2.484×10^{-4}	0.315	2499
	1.3	-	4.78×10^{-5}	1.712×10^{-3}	0.389	1619	8.428×10^{-6}	0.423	295.2
	2.3	-	9.95×10^{-5}	2.946×10^{-3}	0.214	6.333×10^{9}	4.061×10^{-7}	0.646	129.8

The fitted equivalent circuits and parameters of Q235 steel in contaminated soil with different sodium chloride contents at 14, 28, and 60 days are shown in Figure 9 and Table 7. The fitting effect of the LR (QR) (QR) equivalent circuit is good. L is an inductance element, which is caused by the geometric properties of the electrode surface and is not an electrochemical reaction process [38]. The value is very small, and its influence on the total impedance can be ignored. R_s is the resistance of sodium chloride polluted silt soil. It decreases with increasing sodium chloride content in the soil at 14 and 28 days, and R_s increases with increasing corrosion time. However, at 60 days, R_s decreases to 10^{-5}; at this time, corrosion may progress violently. R_{ct} is the charge transfer resistance, and R_{cp} is the resistance of the corrosion product. When steel is buried in soil with a sodium chloride content of 2.3% for 14 days, both values are the maximum of all contents, reaching 2008 Ω·cm^2 and 1971 Ω·cm^2, respectively, which indicates that the charge transfer between the electrode and electrolyte contact surface is extremely difficult. This process seriously hinders the passage of ions. A large number of corrosion products appear on the surface of Q235 steel, which shows obvious passivation with the measured polarization curve. R_{ct} and R_{cp} both decrease at 28 days, and the value for the 2.3% sodium chloride content is the smallest at this time, which is due to the further oxidation of corrosion products into non-corrosive products. The values of R_{ct} and R_{cp} at 60 days both increase compared to 28 days, which also corresponds to the measured polarization curve results. Q_{cp} and Q_{dl} are the corrosion product layer capacitance and the electric double layer capacitance respectively. Due to the "dispersion effect", the constant phase element is used instead. The value of Q_{cp} is close to 1 at 14 and 28 days, which is close to the ideal capacitance, indicating that a relatively dense and uniform corrosion product layer has been formed on the surface of Q235 steel. Eq. (14) for calculating the total impedance of Q235 steel in sodium chloride contaminated soil is derived from Eqs. (12) and (13).

$$Z = R_s + \frac{Z_{cp}R_{cp}}{Z_{cp} + R_{cp}} + \frac{Z_{dl}R_{ct}}{Z_{dl} + R_{ct}}$$

Eq. (12)

$$Z_{cp} = \left[Y_{cp} \left(j\omega \right)^{n1} \right]^{-1}, \; Z_{ct} = \left[Y_{ct} \left(j\omega \right)^{n2} \right]^{-1}$$

Eq. (13)

$$Z = R_s + \frac{R_{cp}}{R_{cp} Y_{cp} \left(\omega j \right)^{n1} + 1} + \frac{R_{ct}}{R_{ct} Y_{Ql} \left(\omega j \right)^{n2} + 1}$$

Eq. (14)

In Eqs. (9), (10) and (11), Z_{cp} and Z_{dl} are the impedances of constant phase elements and corrosion products, and Y_{cp} and Y_{Ql} are constants independent of frequency.

3.4 Macro and microanalysis of Q235 steel corrosion over 60 days

Figure 10. Macro-images of the corrosion of Q235 steel in 0%(a), 0.3%(b), 1.3%(c), and 2.3%(d) sodium chloride silt soil for 60 days

Macro-images of Q235 steel after being buried in 0%, 0.3%, 1.3%, and 2.3% sodium chloride silt for 60 days are shown in Figure 10. As the content of sodium chloride in the soil increases, the corrosion area of Q235 steel continues to expand, the degree of corrosion continues to deepen, and the Q235 steel sheets in the soil with 1.3% and 2.3% sodium chloride have been fully corroded [39]. There are only red-brown corrosion products on the surface of the steel sheet in the uncontaminated soil, and a white corrosion product film also appears on the surface of the steel sheet in 0.3% soil. Sodium chloride precipitated in the soil and adhered to the surface of the steel specimen. The surface of the steel sheet in 1.3%, and 2.3% sodium chloride soil was covered by corrosion products. In particular, when the steel sheet was buried in silt containing 2.3% sodium chloride, there was a layer of obvious dark red-brown corrosion product on its surface. The process of corrosion is mainly caused by Eqs. (15) and (16):

$$3Fe + 4H_2O \rightarrow Fe_3O_4 + 8H^+ + 8e$$

Eq. (15)

$$2Fe + 2H_2O \rightarrow \gamma - Fe_2O_3 + 6H^+ + 6e$$

Eq. (16)
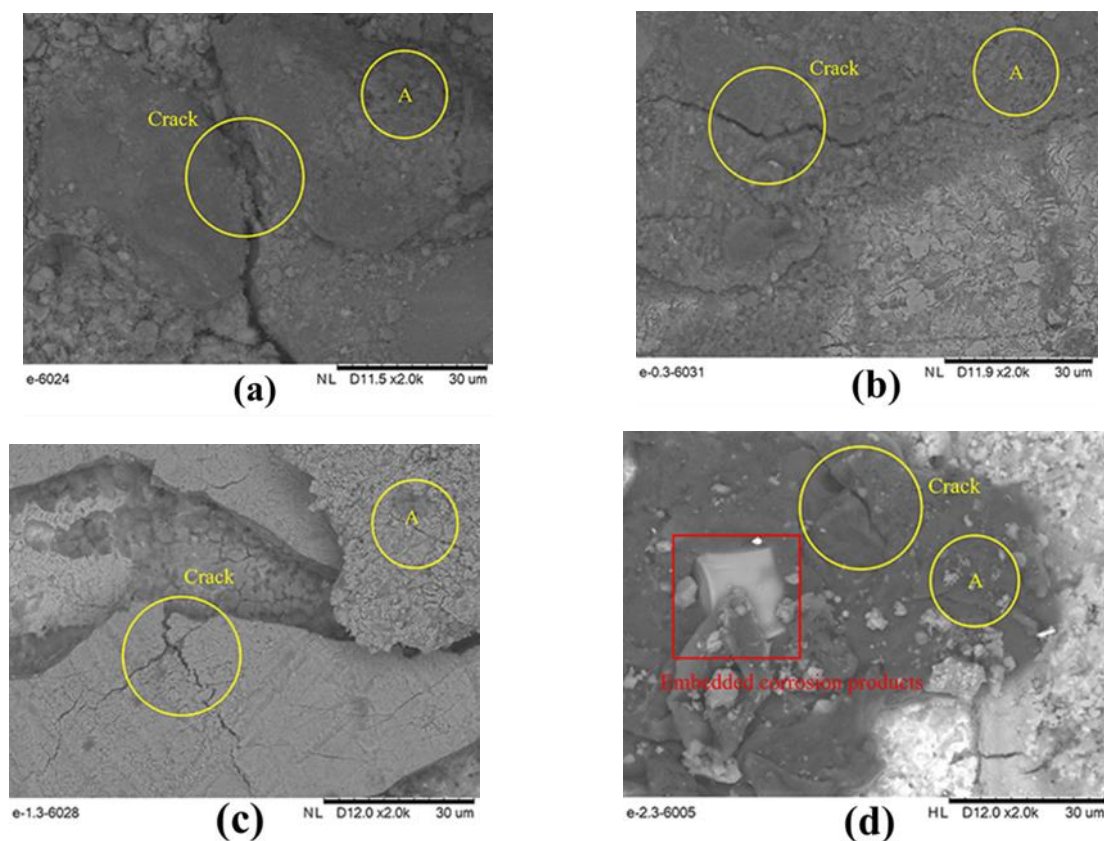
Figure 11. Microscopic images of Q235 steel in 0%(a), 0.3%(b), 1.3%(c), and 2.3%(d) sodium chloride silt soil for 60 days

Microscopic images of Q235 steel after being buried in 0%, 0.3%, 1.3%, and 2.3% sodium chloride silt for 60 days are shown in Figure 11. Observing the microscopic morphology of the steel sheet by a scanning electron microscope, we found that all of the corrosion products have cracks on the surface, and the ions can still reach the surface of the steel sheet through the cracks to cause the test piece to corrode [40]. Therefore, although the measured polarization curve is passivated, the corrosion products decrease the corrosion rate, but corrosion is still ongoing. The corrosion products of the steel sheet in the soil with a content of 1.3% sodium chloride are layered, indicating that several layers of corrosion products have appeared on the surface of the specimen under continuous corrosion. From the microscopic image of the steel sheet buried in 2.3% sodium chloride soil, it can be seen that a solid corrosion product is deeply embedded on the surface of the next layer of corrosion product (see Figure 11 (d)), and the surrounding colour is obviously darker, indicating that a dense corrosion product layer has formed on the surface of the Q235 steel specimen at this time. EDS analysis was performed on area A marked in Figure 11. The element composition of the steel surface after being buried in 1.3% sodium chloride silt for 60 days was obtained by EDS analysis (see Figure 12) and is given as O: Si: Fe: C: Ca: Al=8: 14: 6: 20: 13. The main chemical elements and their mass percentages analysed by EDS are shown in Figure 13. Among them, Si and Ca mainly come from the soil, C and Al come from the Q235 steel itself, and the Fe and O here are mainly from corrosion products. It is obvious that Q235 steel produces

more Fe in contaminated sodium chloride soil than in uncontaminated soil containing. The Fe element content produced by Q235 steel with a 2.3% sodium chloride content is the highest, which is approximately 7 times the mass percentage of the unpolluted soil, indicating that the sodium chloride solution promotes the process of corrosion.
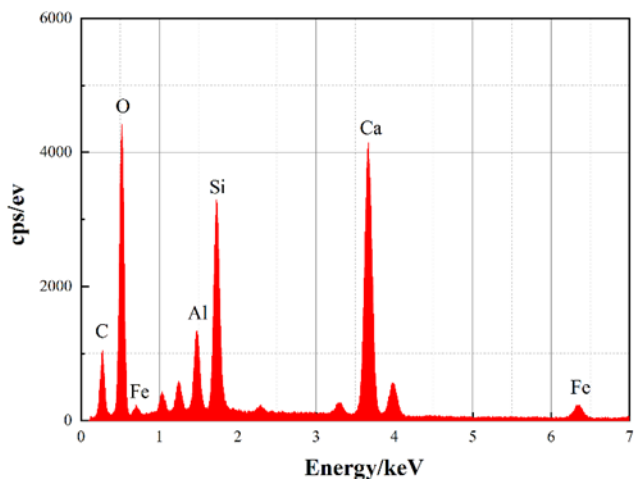
Figure 12. EDS spectrum of the corrosion product layer of Q235 steel in 1.3% sodium chloride contaminated soil after 60 days of corrosion
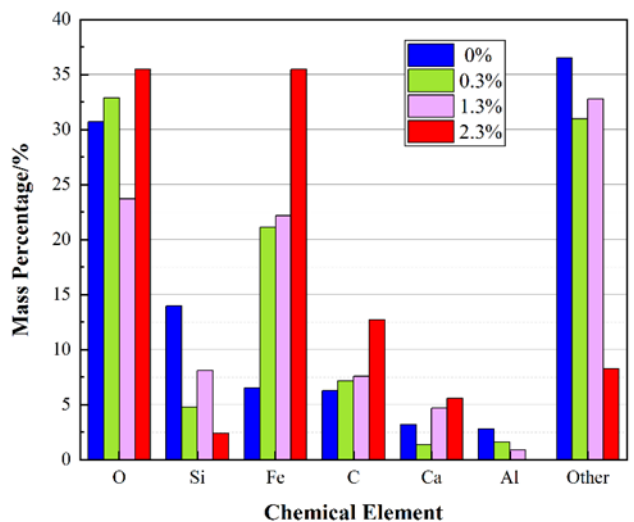
Figure 13. Mass percentages of the main chemical elements on the surface of Q235 steel in 0%, 0.3%, 1.3%, and 2.3% sodium chloride silt corrosion for 60 days

4. CONCLUSIONS

(1) The sodium chloride solution promoted the conductivity of the soil and increased the corrosiveness of the soil. Contaminated soil with a 2.3% sodium chloride content has the strongest

conductivity and the strongest corrosiveness. The resistance R_L of the electrolyte in the pore solution of soil particles in the uncontaminated silt was approximately 27 times compared with the resistance for the soil polluted of with 2.3% sodium chloride.

(2) The corrosion of Q235 steel in the soil was a continuous and changing process. The thermodynamic trend of corrosion changed with the continuous production and oxidation of corrosion products. The corrosion rate of Q235 steel in uncontaminated soil will decrease with increasing burying time. However, under the same number of corrosion days, when the sodium chloride content in the soil reached a certain level, the soil conductivity increased with increasing sodium chloride content in the soil, and the I_{corr} and corrosion rate of Q235 steel also increased. When the corrosion reached 60 days, the I_{corr} and corrosion rate of Q235 steel showed an obvious increasing trend with increasing sodium chloride content in the soil, and extremely serious corrosion occurred in the contaminated soil containing sodium chloride.

(3) The fitting showed that the equivalent circuit of Q235 steel in uncontaminated soil was R (CR (QR)) (CR), the equivalent circuit in contaminated soil containing sodium chloride was LR (QR) (QR), and the deduced total impedance formula was obtained. By analysing the fitted parameters, the corrosion process of Q235 steel was studied.

(4) The corrosion area and degree of corrosion on the surface of the Q235 steel specimen continued to expand with increasing the sodium chloride content in the soil. Local corrosion occurred on the surface of the steel specimen in the uncontaminated soil, and 0.3% sodium chloride polluted silt. When the contents of sodium chloride in the soil were 1.3% and 2.3%, the surface of the steel sample was completely corroded, and the corrosion products were reddish-brown, mainly unstable oxide Fe_3O_4 and corrosion-resistant γ-Fe_2O_3. The micrograph showed that the surface of the steel sample was covered by multiple layers of corrosion products, forming a dense layer of corrosion products.

References

1. R. Martins-Noguerol, J. Cambrollé, J. M. Mancilla-Leytón, A. Puerto-Marchena, S. Muñoz-Vallés, M. C. Millán-Linares, F. Millán, E. Martínez-Force, M. E. Figueroa, J. Pedroche, and A. J. Moreno-Pérez, *Food Chem.*, 352 (2021) 129370.
2. H. M. Ezuber, A. Alshater, S. M. Zakir Hossain, and Ali El-Basir, *Arabian J. Sci. Eng.*, 46(7) (2021) 6177.
3. L. Quej-Aké, N. Nava, M. A. Espinosa-Medina, H. B. Liu, J. L. Alamilla, and E. Sosa, *Corros. Eng., Sci. Technol.,* 50(4) (2015) 311.
4. X. G. Li, D. W. Zhang, Z. Y. Liu, Z. Li, C. W. Du, and C. F. Dong, *Nature*, 527(7579) (2015) 441.
5. R. Z. Xie, Z. G. Chen, C. Feng, B. He, F. L. Ma, P. J. Han and Y. F. Chen., *Mater. Test.*, 60(9) (2018) 841.
6. W. Wei, X. Q. Wu, W. Ke, S. Xu, B. Feng, and B. T. Hu, *J. Mater. Eng. Perform.*, 25(2) (2016) 518.

7. X. R. Li, X. T. Wang, L. Y. Wang, Y. Y. Sun, B. B. Zhang, H. L. Li, Y. L. Huang, and B. R. Hou, *J. Mater. Eng. Perform.*, 28(4) (2019) 2327.
8. R. N. Deo and J. P. Cull, *Geotech. Test. J.*, 38(6) (2015) 965.
9. A. Yajima, H. Wang, R. Y. Liang, and H. Castaneda, *Int. J. Pressure Vessels Pip.*, 126 (2015) 37.
10. I. S. Cole and D. Morney, *Corros. Sci.*, 56 (2012) 5.
11. X. L. Zuo, B. Xiang, X. Li, and Z. D. Wei, *J. Mater. Eng. Perform.*, 21(4) (2012) 524.
12. Y. C. Zhu, G. M. Liu, X. Liu, F. Pei, X. Tian, and H. Y. Gan, *Mater. Mech. Eng.*, 43(10) (2019) 15.
13. L. Xu, X. J. Zhou, P. H. Zheng, J. P. Wu, and J. Wu, *Mater. Prot.*, 53(6) (2020) 50.
14. Y. F. Wang, G. X. Cheng, W. Wu, Q. Qiao, Y. Li, and X. F. Li, *Appl. Surf. Sci.*, 349 (15) (2015) 746.
15. Z. M. You, Y. M. Lai, H. Y. Zeng, and Y. H. Yang. *Constr. Build. Mater.*, 238 (2020) 117762.
16. K. Yin, H. W. Liu, and Y. F. Cheng. *Corros. Sci.*, 145 (2018) 271.
17. A.I.M. Ismail and A. M. El-Shamy, *Appl. Clay Sci.*, 42(3) (2009) 356.
18. M. H. Xu, Q. Zhang, Z. Wang, J. M. Liu, and Z. Li. *Corrosion*, 73(3) (2017) 290.
19. M. C. Yan, C. Sun, J. Xu, J. H. Dong, and W. Ke, *Corros. Sci.*, 80 (2014) 309.
20. M. Barbalat, L. Lanarde, D. Caron, M. Meyer, J. Vittonato, F. Castillon, S. Fontaine, and P. Refait, *Corros. Sci.*, 55 (2012) 246.
21. H. W. Liu and Y. F. Cheng, *Electrochim. Acta*, 253 (2017) 368.
22. S. R. Wang, C. W. Du, X. G. Li, Z. Y. Liu, M. Zhu, and D. W. Zhang, *Prog. Nat. Sci.*, 25(3) (2015) 242.
23. J. Xu, Y. L. Bai, T. Q. Wu, M. C. Yan, C. K. Yu, and C. Sun, *Eng. Fail. Anal.* 100 (2019) 192.
24. I. M. Gadala and A. Alfantazi, *Corrosion Sci.*, 82 (2014) 45.
25. T. Q. Wu, J Xu, C. Sun, M. C. Yan, C. K. Yu, and W. Ke, *Corros. Sci.*, 88 (2014) 291.
26. J. Fu, F. Pei, Z. P. Zhu, Z. H. Tan, X. Tian, R. J. Mao, and L. J. Wang, *Anti-Corros. Methods M*ater. 60(3) (2013) 148.
27. W. Muhammad, S. Shahrukh, N. M. Mubarak, Inamuddin, and A. M. Asiri, *Environ. Chem. Lett.*, 16(3) (2018) 861.
28. D. Wei and P. Wang, *Procedia Engineering,* 210(2017) 79.
29. B. L. Lin, X. Y. Lu, and L. Li, *J. Wuhan Univ. Technol.-Mat. Sci. Edit.*, 26(6) (2011) 1152.
30. Z. W. Chen, P. J. Han, B. He, F. N. Sun, X. L. Bai, X.Y Liu and Y.T Wang, *Int. J. Electrochem. Sci.*, 16 (2021) in press.
31. P. Han, P. J. Han, Y. B. Yan, and X. H. Bai, *Int. J. Electrochem. Sci.*, 14(3) (2019) 3138.
32. X. J. Li, X. Wang, Q. Zhao, Y. Y. Zhang and Q. X. Zhou, *Sensors,* 16(5) (2016). 625
33. F. N. Sun, R. Z. Xie, B. He, Z. W. Chen, X. L. Bai and P. J. Han, *Int. J. Electrochem. Sci.*, 16(1) (2021).
34. Y. Liu, X. H. Tong, B. G. Li, Y. G. Wang and L. S. Zhu, *Advanced Materials Research*, 591 (2012) 1046.
35. W. R. Osorio, L. C. Peixoto and A. Garcia, *Mater. Corros.,* 61(5) (2010) 407.
36. H. Y. Tang, G. L. Song, C. N. Cao, and H. C. Lin, *Corros. Sci. Prot. Technol.,* 7(4) (1995) 285.
37. K. C. Lv, S. Xu, L. L. Liu, X. M, Wang, C. Li, T. Q. Wu and F. C. Yin, *Int. J. Electrochem. Sci.*, 15(6) (2020) 5193.
38. B. He, P. J. Han, C. H. Lu and X. H. Bai, *Eng. Fail. Anal.,* 58(1) (2015) 19.
39. S. Q. Chen and D. Zhang, *Corros. Sci.*, 148 (2019) 71.
40. L. J. Shi, Y. W. Song, K. H. Dong, D. Y. Shan and E. H. Han, *Corrosion Sci.*, 184 (2021) 109400